*J. Fluid Mech.* (2010), *vol.* 647, *pp.* 91–103.  
doi:10.1017/S0022112009994046

# Effect of gravity on the stability of thermocapillary convection in a horizontal fluid layer

CHO LIK CHAN AND C. F. CHEN†

Department of Aerospace and Mechanical Engineering, The University of Arizona, Tucson, AZ 85721, USA

(Received 24 July 2009; revised 14 December 2009; accepted 15 December 2009)

Smith & Davis (*J. Fluid Mech.*, vol. 132, 1983, pp. 119–144) considered the stability of thermocapillary convection in a horizontal fluid layer with an upper free surface generated by a horizontal temperature gradient. They showed that for a return-flow velocity profile, the convection will become unstable in the hydrothermal mode with waves propagating upstream obliquely. Their findings provided a theoretical explanation for the defects often found in crystals grown by the floating-zone technique and in thin-film coating processes. Their predictions were verified experimentally by Riley & Neitzel (*J. Fluid Mech.*, vol. 359, 1998, pp. 143–164) in an experiment with 0.75 mm thick layer of silicone oil. Their results with 1 and 1.25 mm thick layers show that as the thickness of the layer is increased, the angle of propagation, the frequency of oscillation and the phase speed of the hydrothermal wave instability decrease, while the wavelength stays nearly constant. We have extended the linear stability analysis of the problem with the effect of gravity included. It is found that when the Grashof number $Gr$ is increased from zero, the angle of propagation first increases slightly, reaches a maximum and then decreases steadily to zero at $Gr = 18$. The phase speed, the frequency of oscillation and the wavelength of the instability waves all decrease with increasing Grashof number. For $Gr$ larger than 18, there is the onset of the instability into travelling transverse waves. We have also carried out energy analysis at the time of the instability onset. It is found that the major contribution to the energy of the disturbances is from the surface-tension effect. As the gravitational effect is increased, there is a reduction in the kinetic energy supply to sustain the motion of the disturbances. We also found that it requires more kinetic energy to sustain the hydrothermal mode of instability than that required for the travelling transverse mode of instability. As a result, with increasing Grashof number, the kinetic energy available for the disturbances decreases, causing the angle of propagation to gradually decrease until finally reaching zero at $Gr = 18$.

## 1. Introduction

The stability of surface-tension-driven convection generated by a constant horizontal temperature gradient in an infinite plane fluid layer with a free upper surface has been studied by Smith & Davis (1983). Their results show that the most critical instability is in the form of hydrothermal waves (HTWs) that travel upstream obliquely. The

† Email address for correspondence: chen@ame.arizona.edu

angle of propagation depends on the Prandtl number of the fluid. For the case in which there is no heat transfer in the vertical direction through the fluid layer, it decreases from 80° for $Pr = 10^{-3}$ to 20° for $Pr = 10$. They also showed that with heat transfer, the flow becomes more stable. Gershuni *et al.* (1992) studied the stability of such a fluid layer in the presence of gravity. The range of Prandtl numbers considered is from $10^{-3}$ to 10. The temperature of the fluid at the top free surface is maintained at the same value as that at the bottom rigid boundary by vertical heat transfer. As a result, when the surface-tension effect is small as compared with the gravitational effect, there is an inflexing point in the velocity profile near the top free surface, and there are two regions of unstable temperature distributions, one each near the top and bottom boundaries. For such a layer, the critical instability is in the hydrodynamic or the inviscid mode for $Pr \leqslant 0.045$, in the three-dimensional oscillating mode for $0.045 \leqslant Pr \leqslant 0.85$ and in the steady longitudinal mode due to Benard convection for $Pr \geqslant 0.8$. Garr-Peters (1992) considered the stability of the fluid layer with the free surface facing either upward or downward. The Prandtl number range considered is $0.01 \leqslant Pr \leqslant 10$. The longitudinal and transverse modes of instability are considered in part 1 and the oblique mode in part 2 of Garr-Peters (1992). Critical conditions for the onset of instabilities are shown as functions of $Pr$ with the Bond number, the ratio of the surface-tension and gravitational effects, as a parameter.

Parmentier, Regnier & Lebon (1993) carried out stability analysis of convection in a fluid layer both under buoyancy alone and under the combined effects of buoyancy and surface tension. The Prandtl numbers of the fluids considered are from 0.01 to 7, and there is no vertical heat transfer through the top and bottom boundaries. For buoyancy convection of fluids with $Pr \geqslant 2.6$, the flow is unconditionally stable. For fluids with $Pr$ less than 2.6, the instability is in the form of propagating HTWs. For $0.01 < Pr < 0.4$, the waves consist of nearly longitudinal rolls propagating with near-90° angle. For $0.4 < Pr < 2.6$, the propagation angle decreases to 0° at $Pr = 2.6$. With combined forcing by gravity and surface tension for fluids with $Pr > 2.6$, surface tension is the main cause of instability. For $Pr = 7$, as the Rayleigh number is increased, the angle of propagation of the HTWs decreases continuously, and eventually it is reduced to zero, with the instability motion consisting of travelling transverse convection rolls. Mercier & Normand (1996) carried out linear stability analysis in an effort to explain the experimental results of Daviaud & Vince (1993). It was shown in their experiment with water that as the fluid layer thickness is increased, the instability transitions from travelling waves into stationary rolls. Mercier & Normand (1996) showed that such transition is possible by introducing vertical heat transfer through the upper free surface by the use of a Biot number in the boundary condition. For a given value of the Biot number, a limiting ratio of the Marangoni number to the Grashof number can be determined such that when the limit is exceeded, the stationary mode of the instability will transition to the oscillating mode. However, to effect the transition as observed in the experiment would require the Biot number to exceed 70, an unreasonably large amount of heat transfer. The discrepancy was attributed to the limited lateral extend of the experimental tank. Burguete *et al.* (2001) conducted experiments with $Pr = 10$ silicone oil in a rectangular tank with different aspect ratios. The depth of the fluid layer varied from 1 to 10 mm. Their results show that the onset of the instability is into oblique travelling waves in layers of small depths and into stationary longitudinal rolls in layers of larger depths. The transition phenomenon is in general agreement with the theoretical predictions of Mercier & Normand (1996).

The experiments of Riley & Neitzel (1998) were carried out in silicone oil with the Prandtl number of 13.9. A total of nine experiments were conducted in layers of depths increasing from 0.75 to 2.50 mm. In the thinnest layer of 0.75 mm, instability in the hydrothermal mode was observed, and the angle of propagation compares well with the predictions of Smith & Davis (1983). HTWs were also detected in two thicker layers, 1.0 and 1.25 mm. However, in the 1.25 mm layer, HTW instability was transitioned from steady multi-cell instability which had onset at a lower Marangoni number. In the six thicker layers, no HTW instability was observed. The instability motion consisted of steady multi-cells. Even with the limited amount of data on HTW instability, the results of Riley & Neitzel (1998) indicate the changes in the characteristics of the instabilities as the gravitational effect is increased and provide a basis for comparison with the results of linear stability analysis with the effect of gravity included. In the current paper, we report the results of such a stability analysis.

## 2. Equations for linear stability analysis and energy balance

The idealized model of the problem is the convection in a horizontal fluid layer with an upper free surface contained in a long tank. Convection is driven by a temperature difference maintained at the two ends, with the left end being cooler. It is assumed that a constant temperature gradient $\gamma$ is maintained in the central portion of the fluid away from the two ends. The origin of the coordinate system is at the centre of the tank with the $x$-axis in the direction of the positive temperature gradient and the $z$-axis pointing vertically upwards. To write down the basic equations in non-dimensional terms, we use the thickness $d$ of the layer for the scale length, $d^2/\nu$ for time where $\nu$ is the kinematic viscosity, $\nu/d$ for velocity, $\rho_0(\nu/d)^2$ for pressure and $\gamma d$ for temperature.

For a Boussinesq fluid, the continuity, momentum, energy and state equations are

$$\nabla \cdot \boldsymbol{V} = 0, \tag{1}$$

$$\partial \boldsymbol{V}/\partial t + (\boldsymbol{V} \cdot \nabla)\boldsymbol{V} = -\nabla p - k\, GrT + \nabla^2 \boldsymbol{V}, \tag{2}$$

$$\partial T/\partial t + (\boldsymbol{V} \cdot \nabla)T = Pr^{-1}\nabla^2 T, \tag{3}$$

$$\rho = \rho_0[1 - \alpha(T - T_0)]. \tag{4}$$

In the above equations, the Grashof number $Gr = g\alpha\gamma d^4/\nu^2$ with $\alpha = -\rho_0^{-1}\partial\rho/\partial T$; $\boldsymbol{k}$ is the unit vector in the $z$-direction; and the Prandtl number $Pr = \nu/\kappa$, in which $\kappa$ is the thermal diffusivity. The surface tension $\eta$ of the fluid is assumed to vary linearly with $T$:

$$\eta = \eta_0 - \sigma_T(T - T_0) \tag{5}$$

in which $\sigma_T > 0$. The boundary conditions on the velocity are $\boldsymbol{V} = 0$ on all solid surfaces and a balance of shear stresses at the upper free boundary. The top and bottom boundaries are assumed to be insulating with respect to heat. We analyse the stability of the system after steady flow conditions have been established.

In the mid-section of the tank, we assume that the basic flow is parallel, and the temperature $T_b(x, z) = \gamma x + T_b(z)$, where $\gamma$ is the constant temperature gradient. We

obtain the return flow velocity and temperature distributions:

$$\left.\begin{aligned} u_b(z) &= (Gr/192)F_1(z) + (Ma/16)\,F_2(z), \\ F_1(z) &= 32z^3 - 12z^2 - 12z + 1, \\ F^2(z) &= -12z^2 - 4z + 1, \end{aligned}\right\} \tag{6}$$

$$\left.\begin{aligned} T_b(z) &= Pr\,[Gr\,G_1(z) + Ma\,G_2(z)], \\ G_1(z) &= z^5/120 - z^4/192 - z^3/96 + z^2/384 + z/192 - 29/15360, \\ G_2(z) &= -z^4/16 - z^3/24 + z^2/32 + z/32 - 11/768. \end{aligned}\right\} \tag{7}$$

In the above equations, the Marangoni number is defined as $Ma = \gamma\sigma_T d^2/\mu\nu$. We note here that our definition of $Ma$ differs from that of Riley & Neitzel (1998) by a factor $Pr$. In figure 1 we show the basic velocity $u_b(z)$ and temperature $T_b(z)$ at $Gr = 0, 10, 20$ and 40. It shows that the fluid in the layer becomes more stably stratified as $Gr$ is increased.

We analyse the stability characteristics of the parallel flow by assuming small perturbations in the normal mode form:

$$[u'(z), v'(z), w'(z), T'(z)]\exp[\sigma t + \mathrm{i}(A_x x + A_y y)] \tag{8}$$

in which $\sigma = \sigma_r + \mathrm{i}\sigma_i$. When these perturbations are substituted into the governing equations (1)–(3) and higher-order terms are neglected, we obtain the linear stability equations. The perturbation equations in the normal mode form with the primes deleted are

$$\mathrm{i}A_x u + \mathrm{i}A_y v + \mathrm{D}w = 0, \tag{9}$$

$$\sigma u + \mathrm{i}A_x u_b u + w\mathrm{D}u_b = -\mathrm{i}A_x p + \left(\mathrm{D}^2 - A_x^2 - A_y^2\right)u, \tag{10}$$

$$\sigma v + \mathrm{i}A_x u_b v = -\mathrm{i}A_y p + \left(\mathrm{D}^2 - A_x^2 - A_y^2\right)v, \tag{11}$$

$$\sigma w + \mathrm{i}A_x u_b w = -\mathrm{D}p + GrT + \left(\mathrm{D}^2 - A_x^2 - A_y^2\right)w, \tag{12}$$

$$\sigma T + \mathrm{i}A_x u_b T + u + w\mathrm{D}T_b = Pr^{-1}\left(\mathrm{D}^2 - A_x^2 - A_y^2\right)T, \tag{13}$$

with boundary conditions

$$u = v = w = \mathrm{D}T = 0 \quad \text{at} \quad z = -1/2, \tag{14}$$

$$w = \mathrm{D}T = 0, \quad \mathrm{D}u = -\mathrm{i}A_x MaT, \quad \mathrm{D}v = -\mathrm{i}A_y MaT \quad \text{at} \quad z = 1/2. \tag{15}$$

In these equations D denotes $\mathrm{d}/\mathrm{d}z$.

Chebyschev pseudo-spectral collocation method (Canuto *et al.* 1988) was used to solve the eigenvalue problem (9)–(15). The resulting complex matrix eigenvalue problem was solved by using subroutine CQZHES.f, downloaded from netlib (www.netlib.org/toms/535). Quadruple precision was used for all the calculations. The convergence was investigated. It was found that accurate results are obtained by using 64 collocation points.

The neutral point for a set of $Gr$, $Pr$, $A_X$ and $A_Y$ is generated by using Brent's algorithm (Press *et al.* 2007). A coarse grid, typically 0.5 increment, for $A_X \in [0, 10]$ and $A_Y \in [0, 10]$ is first generated. These results allow rough estimates of the local minima. Local minima for $A_x = 0$ and $A_y = 0$ are obtained by repeated refinement of the grid until the increment is less than $1 \times 10^{-4}$.

For the local minimum of the oblique mode in which both $A_x \neq 0$ and $A_y \neq 0$, the procedure is as follows. From the coarse grid results, a $3 \times 3$ grid with a local

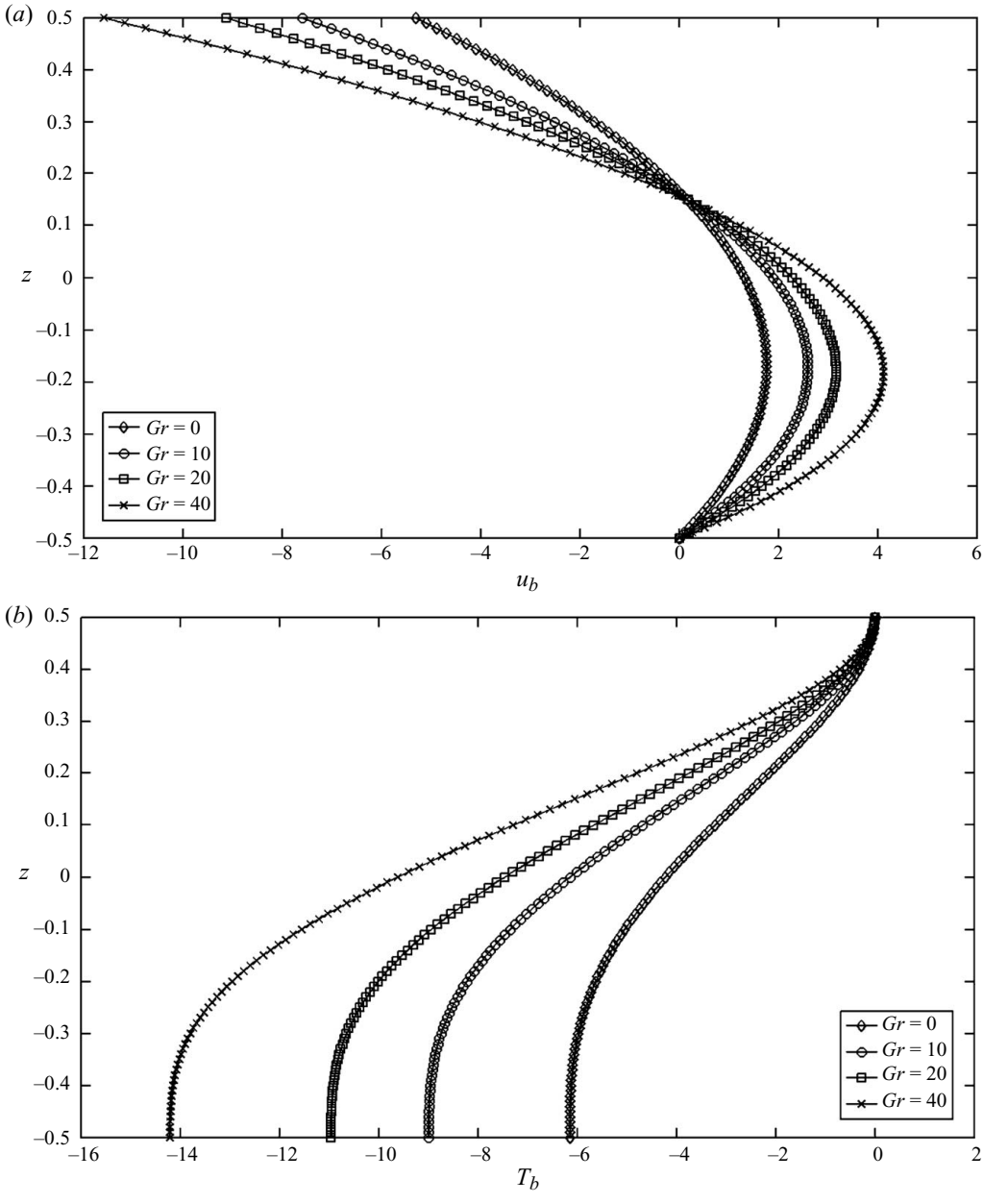


FIGURE 1. Basic velocity and temperature distributions for a fluid with $Pr = 13.9$.

minimum at the centre is identified. Grid refinement by reducing the increment by a factor of 2 is carried out. The reduced $3 \times 3$ grid is re-examined to identify the minimum. If necessary, the reduced $3 \times 3$ grid is shifted to the centre of the minimum. When the minimum is centred, grid refinement is repeated. The process is repeated until the increment is less than $1 \times 10^{-4}$. After the critical point is located, a very coarse grid of points in the $A_X$ and $A_Y$ planes outside the previous coverage area are examined to ensure there are no additional local minima.

Before applying this set of equations to analyse the problem at hand, we validated the equations and the method of solution by applying the method to a thermocapillary convection problem. For a $Pr = 10$ fluid, the solution procedure yielded the following critical conditions: the Marangoni number $Ma = 27.386$, the angle of propagation $\psi = 21.111$, the wavenumber $A_C = 2.565$ and the phase speed = 0.0598. The results of Smith & Davis (1983) for the same case are $Ma = 27.386$, $\psi = 21.05°$, $A_C = 2.565$ and the phase speed = 0.0598. The agreement is very good.

In order to gain a better understanding of the sources of energy that sustain the motion of the instabilities at the time of onset, we examine the energy balance at that time. This is accomplished by summing up the dot products of the perturbation velocity vector and the perturbation momentum equations with $\sigma_r = 0$. Hart (1972) used the same method in examining the instability of motion in a non-rotating Hadley circulation cell. The dot product is defined as $\langle \varphi^*, \psi \rangle = \int_{-1/2}^{1/2} \varphi^* \psi \, \mathrm{d}z$, where the superscript '*' denotes complex conjugate of the function.

The resulting energy balance equation is

$$E_M + E_S + E_T = E_D + E_K \tag{16}$$

in which $E_M$ is the work done by surface tension along the free surface; $E_S$ is the energy generated by the shear of the basic flow; $E_T$ is the potential energy generated by vertical transport of fluids with temperature anomalies due the temperature perturbation and is directly proportional to $Gr$; $E_D$ is the energy of dissipation; and $E_K$ is the kinetic energy of the motion of the perturbations. The mathematical expressions of these energy terms are

$$E_M = \mathrm{i}A_x Ma[(u\,T* - u*\,T)]_{1/2} + \mathrm{i}A_y Ma[(v\,T* - v*\,T)]_{1/2}, \tag{17}$$

$$E_S = -(\langle u, w * \mathrm{D}u_b \rangle + \langle u*, w\mathrm{D}u_b \rangle), \tag{18}$$

$$E_T = Gr(\langle w*, T \rangle + \langle w, T* \rangle), \tag{19}$$

$$E_D = 2(\langle \mathrm{D}u, \mathrm{D}u* \rangle + \langle \mathrm{D}v, \mathrm{D}v* \rangle + \langle \mathrm{D}w, \mathrm{D}w* \rangle), \tag{20}$$

$$E_K = 2\left(A_x^2 + A_y^2\right)(\langle u, u* \rangle + \langle v, v* \rangle + \langle w, w* \rangle). \tag{21}$$

## 3. Results of stability analysis

We apply linear stability analysis to the experiments of Riley & Neitzel (1998) in which the working fluid was 1 cS Dow Corning 200 silicone oil, whose thermophysical properties were tabulated by Sumita & Olson (2003) in their paper on thermal convection experiments in rotating shells. Its Prandtl number is 13.9 at 25°C. The dependence of its surface tension on temperature was measured by Riley & Neitzel (1998) to be

$$\eta(T) = [17.237 - 0.0755(T - T_0)] \ \mathrm{mNm}^{-1} \tag{22}$$

in which $T_0 = 25°\mathrm{C}$. In view of (22), $\sigma_T = 0.0755$ mN $(\mathrm{m\,K})^{-1}$. The linear stability equations are solved for either a given layer thickness or a given Grashof number. It is noted that for a given thickness $d$ of the layer, the Grashof and Marangoni numbers are related by

$$Ma/Gr = \sigma_T/(\rho g \alpha d^2) = \mathrm{const}\ d^{-2}.$$

In either case, the solution yields the critical values of $Gr$, $Ma$, the wavenumber vector $A_C$ with its $x$-component and $y$-component $A_x$ and $A_y$, the angle of wave propagation

| $Gr$ | $Ma$ | $A_x$ | $A_y$ | $A_c$ | $\Psi$, deg | $\sigma_i$ | $\lambda/d$ | $-\sigma_i/A_cMa$ | $\lvert\sigma_i\rvert/2\pi Ma$ |
|---|---|---|---|---|---|---|---|---|---|
| 0.000 | 21.213 | 2.430 | 0.737 | 2.540 | 16.867 | −3.259 | 2.474 | 0.060 | 0.024 |
| 1.823 | 22.829 | 2.382 | 0.853 | 2.530 | 19.709 | −3.448 | 2.484 | 0.060 | 0.024 |
| 2.000 | 22.994 | 2.378 | 0.863 | 2.529 | 19.943 | −3.466 | 2.484 | 0.060 | 0.024 |
| 3.461 | 24.383 | 2.354 | 0.932 | 2.532 | 21.593 | −3.604 | 2.482 | 0.058 | 0.024 |
| 5.936 | 26.769 | 2.419 | 1.018 | 2.624 | 22.827 | −3.731 | 2.394 | 0.053 | 0.022 |
| 7.520 | 28.024 | 2.654 | 0.959 | 2.822 | 19.871 | −3.468 | 2.227 | 0.044 | 0.020 |
| 8.000 | 28.339 | 2.701 | 0.922 | 2.854 | 18.843 | −3.374 | 2.202 | 0.042 | 0.019 |
| 9.306 | 29.140 | 2.771 | 0.847 | 2.898 | 17.000 | −3.184 | 2.168 | 0.038 | 0.017 |
| 10.000 | 29.548 | 2.794 | 0.818 | 2.911 | 16.328 | −3.101 | 2.158 | 0.036 | 0.017 |
| 13.000 | 31.250 | 2.872 | 0.707 | 2.958 | 13.824 | −2.742 | 2.124 | 0.030 | 0.014 |
| 13.766 | 31.672 | 2.897 | 0.669 | 2.973 | 12.994 | −2.630 | 2.113 | 0.028 | 0.013 |
| 15.000 | 32.338 | 2.947 | 0.585 | 3.005 | 11.222 | −2.415 | 2.091 | 0.025 | 0.012 |
| 15.951 | 32.838 | 2.994 | 0.491 | 3.034 | 9.321 | −2.219 | 2.071 | 0.022 | 0.011 |
| 17.135 | 33.443 | 3.058 | 0.312 | 3.074 | 5.828 | −1.944 | 2.044 | 0.019 | 0.009 |
| 17.847 | 33.796 | 3.098 | 0.067 | 3.099 | 1.242 | −1.767 | 2.028 | 0.017 | 0.008 |
| 18.000 | 33.872 | 3.104 | 0.000 | 3.104 | 0.000 | −1.739 | 2.024 | 0.016(5) | 0.008 |
| 19.692 | 34.687 | 3.162 | 0.000 | 3.162 | 0.000 | −1.459 | 1.987 | 0.013 | 0.007 |
| 20.000 | 34.832 | 3.172 | 0.000 | 3.172 | 0.000 | −1.406 | 1.981 | 0.013 | 0.006 |
| 27.381 | 38.107 | 3.393 | 0.000 | 3.393 | 0.000 | −0.069 | 1.852 | 0.001 | 0.000 |
| 27.738 | 38.257 | 3.403 | 0.000 | 3.403 | 0.000 | $0^*$ | 1.846 | $0^{**}$ | $0^{***}$ |
| 30.000 | 39.191 | 3.465 | 0.000 | 3.465 | 0.000 | 0.444 | 1.814 | −0.003 | 0.002 |
| 35.000 | 41.172 | 3.598 | 0.000 | 3.598 | 0.000 | 1.485 | 1.746 | −0.010 | 0.006 |
| 37.300 | 42.048 | 3.659 | 0.000 | 3.659 | 0.000 | 1.991 | 1.717 | −0.013 | 0.008 |
| 40.000 | 43.052 | 3.729 | 0.000 | 3.729 | 0.000 | 2.607 | 1.685 | −0.016 | 0.010 |

TABLE 1. Critical conditions at the instability onset for given Grashof number.

$0^* = 4.21 \times 10^{-5}$, $0^{**} = 6.01 \times 10^{-7}$ and $0^{***} = 3.25 \times 10^{-7}$.

$\psi$ and the non-dimensional time factor $\sigma_i$. These values are listed in table 1. We note here that $\sigma_i$ changes from negative to positive values within the range of Grashof numbers considered. For comparison with the experimental results of Riley & Neitzel (1998), we also show the non-dimensional values of the wavelength $\lambda/d$, frequency $|\sigma_i|\,2/\pi Ma$ ($= fd/U_s$ in Riley & Neitzel 1998) and phase speed $-\sigma_i/A_C Ma$ ($= c/U_s$ in Riley & Neitzel 1998). It is noted that with this definition of the phase speed, a positive value indicates that the waves are moving towards the hot boundary.

The stability results were obtained for $Gr = 0$–40, which is the range of the experimental Grashof numbers (based on the measured temperature gradient along the interface) reported by Riley & Neitzel (1998) for their experiments. From table 1, it is seen that the critical Marangoni number $Ma$ and wavenumber $A_C$ both increase with $Gr$. The angle of wave propagation $\psi$ for the HTW mode of instability first increases from its value at $Gr = 0$, reaches a maximum at $Gr \approx 6$ and then gradually decreases to 0 at $Gr = 18$. For $18 \leqslant Gr \leqslant 40$, the onset of instability is in the form of travelling transverse convection rolls with wave propagation angle $\psi = 0°$. The general decreasing trend of $\psi$ with $Gr$ and the travelling transverse convection rolls at high $Gr$ are similar to the predictions of Parmentier *et al.* (1993) for a $Pr = 7$ fluid. It is also noted that $\sigma_i$ starts out being negative at $Gr = 0$, increases to 0 at $Gr = 27.74$ and becomes positive at higher Grashof numbers. This means that at $Gr = 27.74$, the onset of instability is in the form of stationary transverse convection rolls. But for $Gr > 27.74$, the transverse convection rolls will once again be in the travelling mode in the opposite direction.

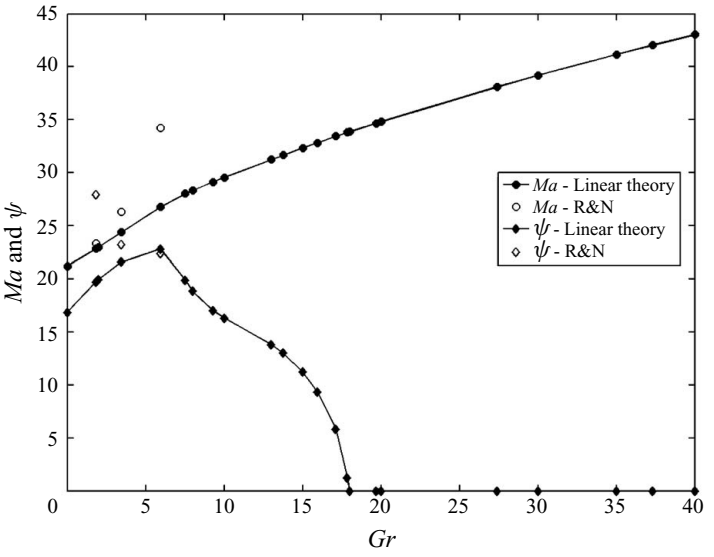


FIGURE 2. Critical Marangoni number and angle of propagation (in degrees) for a fluid with $Pr = 13.9$.

The comparisons between theoretical predictions and the experimental results of Riley & Neitzel (1998) are shown in graphical presentations. In figure 2, the critical Marangoni number and the angle of wave propagation $\psi$ are shown as a function of the Grashof number. The theoretical results show an increasing trend in the critical Marangoni number with the Grashof number. The experimental results for the two thinnest layers show reasonable agreement with the predicted ones, within 8 % of the theoretical values. The theoretical results show that the propagation angle increases from 16.87° at $Gr = 0$ to 22.83° at $Gr = 5.94$ and then decreases steadily to 0° at $Gr = 18$. Thereafter, the angle of propagation remains zero up to $Gr = 40$. The comparison with experimental values is not so good with large discrepancy for the 0.75 mm layer. For the 1.0 mm and 1.25 mm layers, there is reasonable agreement between the theory and the experiment, but bear in mind that for the 1.25 mm layer, HTWs developed from steady multi-cells that have their onset as the initial instability in the experiment. In figure 3, the non-dimensional wavelength $\lambda/d$ is shown as function of the Grashof number. It is seen that $\lambda/d$ stays nearly constant at 2.5 from $Gr = 0$–3.5. It then decreases sharply at first to 2.20 at $Gr = 8$ and more slowly to 1.685 at $Gr = 40$. The experimental values for the two thinnest layers are within 5 % of the predicted values. The variations of non-dimensional phase speed and the frequency with the Grashof number are shown in figure 4. The phase speed decreases from 0.06 at $Gr = 0$ and reaches 0 at $Gr = 27.74$ and furthermore becomes negative at higher $Gr$. Physically, this means a change in the direction of wave motion. The three experimental points of Riley & Neitzel (1998) for both the phase speed and the frequency compare favourably with the theoretical results.

The discrepancies between the experimental results and the predictions of the linear stability analysis may be partially due to (i) the neglect of the lateral boundaries in the stability analysis and (ii) the experimental instabilities that were observed at finite disturbance amplitudes.

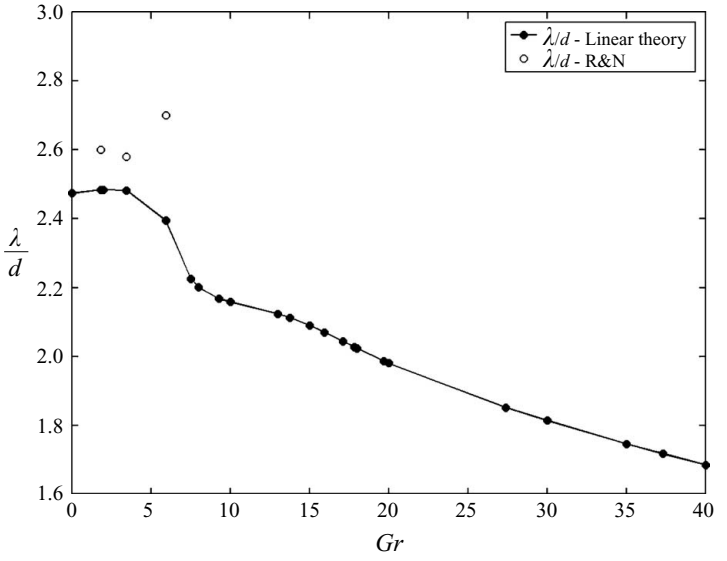


FIGURE 3. Critical non-dimensional wavelength for a fluid with $Pr = 13.9$.

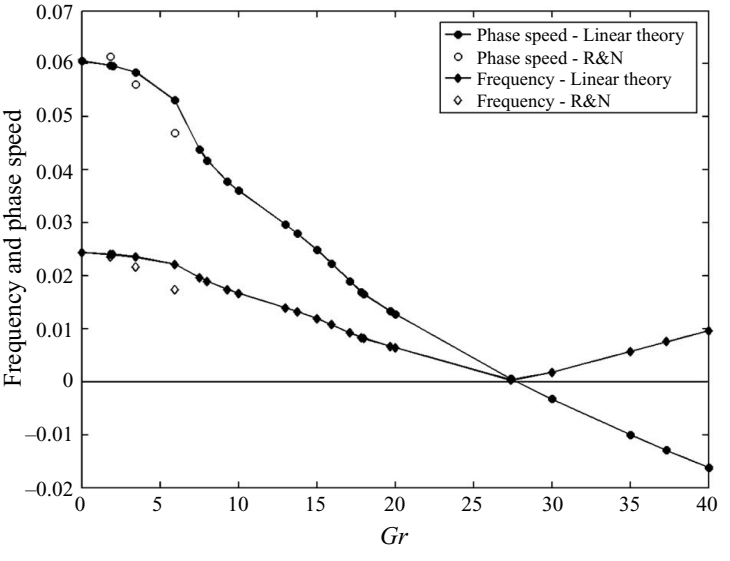


FIGURE 4. Critical values of non-dimensional frequency and phase speed for a fluid with $Pr = 13.9$.

## 4. Results of energy analysis and discussions of the results

In the energy balance equation (16), the term $E_T$ accounts for the conversion of potential energy generated by thermal convection to kinetic energy. We analyse this term in some detail because it is the energy directly contributed by thermal convection to sustain the instability motion. For this purpose, we choose the critical state at a moderate Grashof number $Gr = 10$. In figure 5, the perturbation streamlines at the instability onset is shown along the $x'$-axis in the direction of the wavenumber vector.

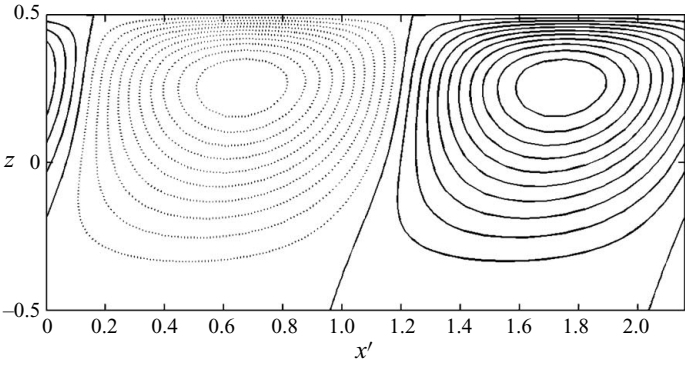


FIGURE 5. Perturbation streamline at instability onset for $Gr = 10$ (——, clockwise; ·····, counterclockwise).

As shown in (19), $E_T$ involves the product of perturbation vertical velocity $w$ and perturbation temperature $T$. The distributions of $w$, $T$ and the product $2Gr(wT)$ in the $x'$–$z$ plane within one wavelength are shown in figure 6. It is seen that $w$ and $T$ are out of phase, resulting in four large regions in the $x'$–$z$ plane with negative values of $2Gr(wT)$. In these regions, either relatively cold fluid is being transported upward, or relatively warm fluid is being transported downward. In either case, work input is required to increase the potential energy of the system. As a result, $E_T$ becomes an energy sink rather than an energy source.

For each of the Grashof numbers considered in the stability analysis, we evaluate the five energy terms shown in (17)–(21). The results are shown in figure 7. Out of the three energy production terms, $E_M$ is the largest; $E_S$ is two orders of magnitude smaller; and $E_T$ has a negative value. The overall effect of increased thermal convection is to stabilize the system. The stabilizing effect is applied directly through the energy sink $E_T$ and indirectly through the decreasing magnitudes of $E_M$ and $E_S$ with increasing Grashof number. The reduction in the magnitudes of $E_M$ and $E_S$ is approximately 40 % from $Gr = 0$ to $Gr = 18$. The magnitude of the negative energy generated by the thermal convection, $E_T$, increases first sharply from zero at $Gr = 0$ to $Gr \approx 6$ and then more slowly to attain its maximum at $Gr \approx 16$. As a result, at $Gr = 18$, the kinetic energy available to sustain the instability motion, $E_K (= 0.0180)$ is reduced by 60 % from its maximum value at $Gr = 0$.

It is reasonable to conjecture that the reduction of kinetic energy available for the instability motion is the cause for the decrease in the propagation angle of HTW instabilities with increasing Grashof number. The propagation angle is reduced eventually to zero at $Gr = 18$, and the instability motion consists of travelling transverse convection rolls. For this conjecture to be true, we need to show that the kinetic energy required to sustain the oblique mode of instability is larger than that for the transverse mode of instability under nearly the same Grashof and Marangoni numbers. We choose the experimental case with the 1.75 mm layer as an example (see table 2). From stability analysis, the critical state is found at $Gr = 13.766$ and $Ma = 31.671$ in the HTW mode with angle of propagation $\Psi = 12.99°$. There is a neighbouring critical state with slightly higher $Gr = 13.785$ and $Ma = 31.715$ for which the instability is in the travelling transverse convection rolls with angle of propagation $\psi = 0°$. Results of energy analysis for these two states, listed in table 2, indeed show that $E_K$ required for the oblique mode is larger than that required for the transverse

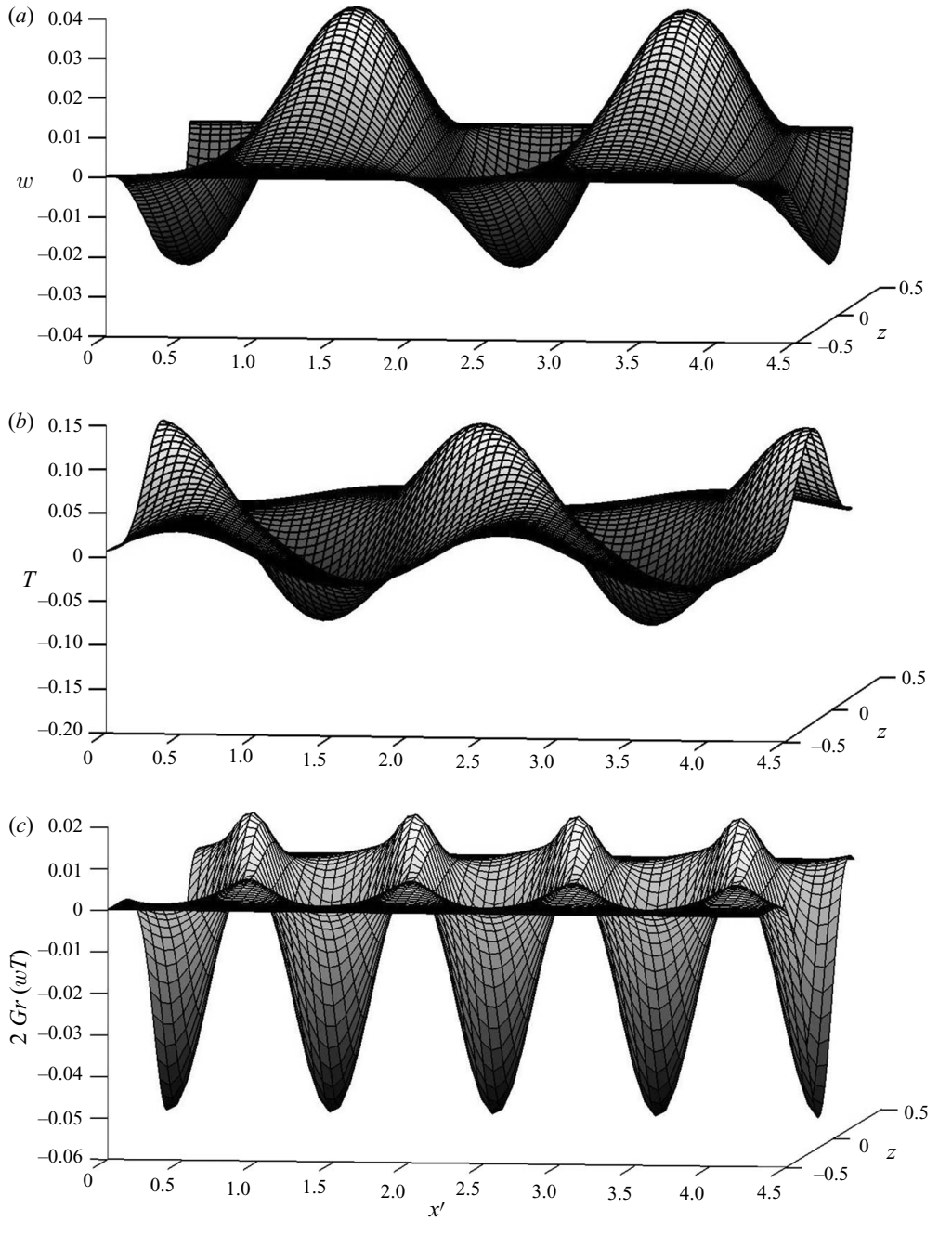


FIGURE 6. Perturbation $w$, $T$ and $2Gr(wT)$ in the $x'$–$z$ plane at the instability onset for $Gr=10$.

mode of instability by about 2 %. By this reasoning, when $E_K$ is reduced below a certain threshold, the onset of the instability will transition from the HTW mode to travelling transverse convection rolls. In the case of silicone oil with $Pr=13.9$, when $E_K$ is reduced to below 0.0180 (the value of $E_K$ for $Gr=18$), the instability onset cannot be in the oblique mode. This argument offers a plausible explanation of the

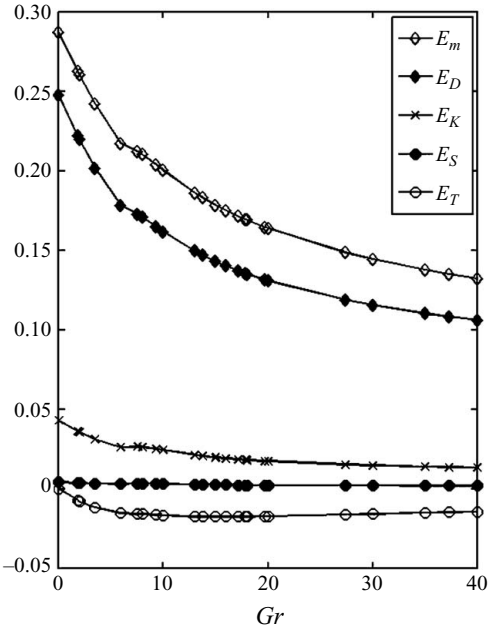


FIGURE 7. Variations of the energy terms $E_M$, $E_D$, $E_K$, $E_S$ and $E_T$ with $Gr$.

| $d$ (mm) | $Gr$ | $Ma$ | $\Psi$ (deg) | $E_m$ | $E_S \times 10^2$ | $E_T \times 10$ | $E_K \times 10$ | $E_D$ |
|---|---|---|---|---|---|---|---|---|
| 1.75 | 13.785 | 31.715 | 0 | 0.1829 | 0.2229 | −0.1791 | 0.2015 | 0.1466 |
| 1.75 | 13.766 | 31.671 | 12.99 | 0.1829 | 0.2530 | −0.1762 | 0.2053 | 0.1468 |

TABLE 2. Comparison of energy terms between the transverse and oblique modes of instability in a 1.75 mm fluid layer.

continued decrease of $\psi$ from $Gr \approx 6$ to reach 0° at $Gr = 18$. However, it does not explain our results that $\psi$ increases initially, reaching a maximum, and then decreases thereafter, while energy analysis results show that $E_K$ decreases continuously from its value at $Gr = 0$. It could be that there also exists a high threshold of $E_K$ above which, regardless of the magnitude of $E_K$, the angle of propagation will increase.

In conclusion, the results of our stability analysis compare reasonably well with the experimental results obtained with great skill and care by Riley & Neitzel (1998). The results of our energy balance analysis carried out at the time of the instability onset show the following: (i) the action of the surface-tension force along the free surface is the major contributor of energy that sustains the instability motion; (ii) in the presence of gravity, part of that energy, which increases with $Gr$, is expended to increase the potential energy of the fluid layer; and (iii) instability in the oblique mode requires more energy than that needed for instability in the transverse mode. These results lead to the conclusion that as the effect of gravity is increased, oblique mode of instability will be replaced by instabilities in the transverse mode. Such mode switching was observed in the experiments of Riley & Neitzel (1998) as the layer thickness was increased.

We thank the referee who furnished us with the critical values of $Ma$, $\psi$, $A_c$, and the phase speed of the hydrothermal wave instability for a $Pr = 10$ fluid as obtained by Smith & Davis (1983).

## REFERENCES

Burguete, J., Mukolobweiz, N., Daviaud, F., Garnier, N. & Chiffaudel, A. 2001 Buoyant-thermocapillary instabilities in extended liquid layers subjected to a horizontal temperature gradient. *Phys. Fluids.* **13**, 2773–2787.

Canuto, C., Hussaini, M. Y., Quarteroni, A. & Zang, T. A. 1988 *Spectral Methods in Fluid Dynamics*. Springer.

Daviaud, F. & Vince, J. M. 1993 Traveling waves in a fluid layer subjected to a horizontal temperature gradient. *Phys. Rev.* E **48**, 4432–4436.

Garr-Peters, J. M. 1992 The neutral stability of surface-tension driven cavity flows subject to buoyant forces. Part 1. Transverse and longitudinal disturbances, and Part 2. Oblique disturbances. *Chem. Engng Sci.* **47**, 1247–1276.

Gershuni, G. Z., Laure, P., Myznikov, V. M., Roux, B. & Shukhovitsky, E. M. 1992 On the stability of plane-parallel advective flows in long horizontal layers. *Microgravity Quart.* **2**, 141–151.

Hart, J. E. 1972 Stability of thin non-rotating Hadley circulation. *J. Atmos. Sci.* **29**, 687–697.

Mercier, J. F. & Normand, C. 1996 Buoyant-thermocapillary instabilities of differentially heated liquid layers. *Phys. Fluids* **8**, 1433–1445.

Parmentier, P. M., Regnier, V. C. & Lebon, G. 1993 Buoyant-thermocapillary instabilities in medium Prandtl-number fluid layers subject to a horizontal temperature gradient. *Intl J. Heat Mass Transfer* **36**, 2417–2427.

Press, W. H., Flannery, B. P., Teukolsky, S. A. & Vetterling, W. T. 2007 *Numerical Recipes,* 3rd edn. Cambridge University Press.

Riley, R. J. & Neitzel, G. P. 1998 Instability of thermocapillary–buoyancy convection in shallow layers. Part 1. Characteristics of steady and oscillatory instabilities. *J. Fluid Mech.* **359**, 143–164.

Smith, M. K. & Davis, S. H. 1983 Instabilities of dynamic thermocapillary liquid layers. Part 1. Convective instabilities. *J. Fluid Mech.* **132**, 119–144.

Sumita, I. & Olson, P. 2003 Experiments on highly supercritical thermal convection in a rapidly rotating hemispherical shell. *J. Fluid Mech.* **492**, 271–287.